DNA Nanotechnology

DOI: 10.1002/anie.200806000

Icosahedral DNA Nanocapsules by Modular Assembly**

*Dhiraj Bhatia, Shabana Mehtab, Ramya Krishnan, Shantinath S. Indi, Atanu Basu, and Yamuna Krishnan**

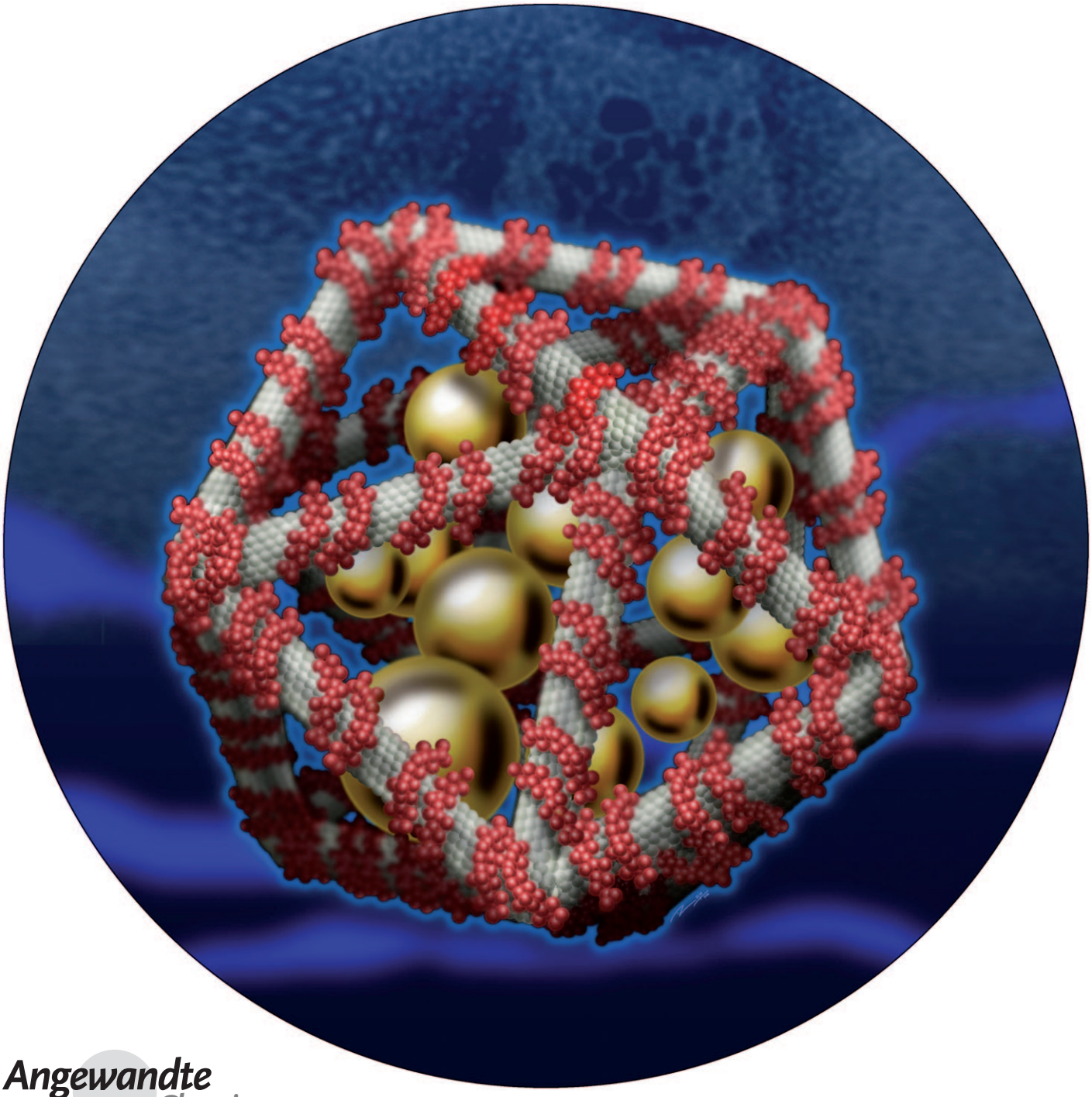

The construction of well-defined 3D architectures is one of the greatest challenges of self-assembly. Nanofabrication through molecular self-assembly has resulted in the formation of DNA polyhedra with the connectivities of cubes,[1] tetrahedra,[2,3] octahedra,[4,5] dodecahedra,[3] and buckminsterfullerene.[3] DNA polyhedra could also function as nanocapsules and thereby enable the targeted delivery of entities encapsulated from solution. Key to realizing this envisaged function is the construction of complex polyhedra that maximize encapsulation volumes while preserving small pore size. Polyhedra based on platonic solids are most promising in this regard, as they maximize encapsulation volumes. We therefore constructed the most complex DNA-based platonic solid, namely, an icosahedron, through a unique modular assembly strategy and demonstrated this functional aspect for DNA polyhedra by encapsulating gold nanoparticles (GNPs) from solution.

This modular assembly strategy to access complex polyhedra involves a stepwise amalgamation of discrete modules obtained from degenerate components. DNA icosahedra may be constructed from three distinct five-way-junction (5WJ)[6,7] components **V**, **U**, and **L**, with programmable overhangs (Figure 1a; see Table 1 in the Supporting Information for sequences). Each 5WJ module, **V**, **U**, and **L**, is constructed from equimolar amounts of the respective five phosphorylated single strands (Figure 2a; see also Figure 2 in the Supporting Information). At 20 μM, **V** was shown to form a complex with **L** in a 1:5 ratio (Figure 2a,b). The complementary module $\mathbf{VU_5}$ was synthesized similarly from components **V** and **U** (see Figure 3a in the Supporting Information). At this stage, contiguously hybridized strands in $\mathbf{VU_5}$ and $\mathbf{VL_5}$ were ligated chemically with *N*-cyanoimidazole (NCI)[8,9] to enhance stability.

When 5WJs of **U** attached to 3.5 nm gold nanoparticles were complexed with **V** in a 1:5 ratio and investigated by electron microscopy, several pentagonal arrangements of gold nanoparticles were observed in the [1:5] complex $\mathbf{VU_5}$ (Figure 2c,d; see also Figure 3 in the Supporting Information). The average center-to-center distance between two gold nanoparticles that mark adjacent vertices ("a") and non-adjacent vertices ("b"; see Figure 3 in the Supporting Information) in these pentagonal arrangements of $\mathbf{VU_5}$ were $a = 8.8 \pm 1$ nm ($n = 36$) and $b = 13.7 \pm 1.7$ ($n = 12$). This result is consistent with the theoretical distances ($a = 8.3$ nm, $b = 13.4$ nm) in the proposed half-icosahedral, compacted, cup-shaped arrangements resulting from recognition between complementary overhangs $\mathbf{U}_5$ and $\mathbf{U}_2$ of adjacent **U** 5WJs in the complex $\mathbf{VU_5}$.

The two different modular assemblies, $\mathbf{VU_5}$ and $\mathbf{VL_5}$, with ten identical overhangs each (the overhangs are complementary in the two assemblies), were shown to complex with each other in a 1:1 ratio. The contiguous termini were ligated again with NCI to yield a complex **I** with a 2:5:5 **V**/**U**/**L** stoichiom-

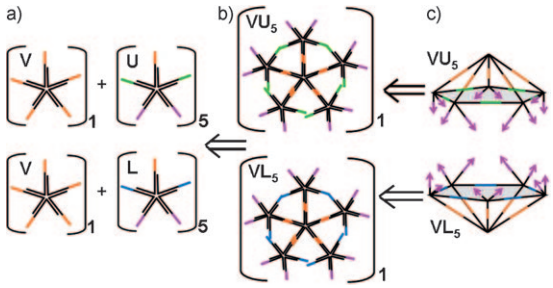

Figure 1. Retrosynthetic strategy for the construction of the DNA icosahedron: The icosahedron **I** is constructed from two half-icosahedra, $\mathbf{VU_5}$ and $\mathbf{VL_5}$, which in turn are formed from two types of 5WJ, **V** and **U**/**L**. a) The 5WJs **V**, **U**, and **L** are shown. The heavy black lines represent double-stranded regions, and the complementary overhangs are color-coded. b) Each half is formed from a central vertex 5WJ, **V**, and five equivalents of the 5WJ **U** or **L**. c) The complex structure, **I**, is formed by the addition of an upper ($\mathbf{VU_5}$) to a lower half ($\mathbf{VL_5}$) in a 1:1 ratio.

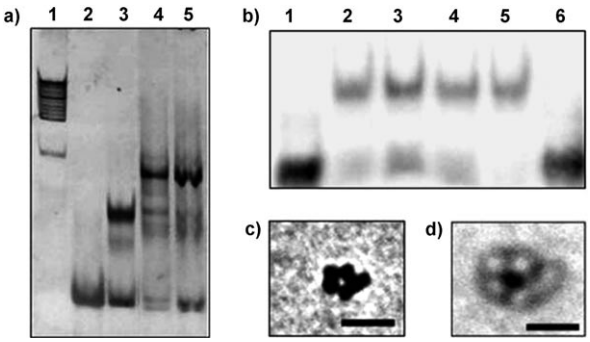

Figure 2. Gel electrophoretic images showing the formation of the complexes at various stages of assembly. a) PAGE (10%) showing the formation of the 5WJ **V** and the formation of the [1:5] complexes $\mathbf{VU_5}$ and $\mathbf{VL_5}$ from 5WJs. Lane 1: DNA marker; lane 2: V1 oligonucleotide; lane 3: 5WJ **V**; lane 4: $\mathbf{VU_5}$; lane 5: $\mathbf{VL_5}$. b) Gel electrophoresis showing the formation of the [1:5] complex $\mathbf{VL_5}$ in the indicated stoichiometry. The radiolabeled 5WJ **V** was complexed with the unlabeled 5WJ **L** at different ratios. Samples were then subjected to electrophoresis on 10% native PAGE in TBE buffer and visualized with PhosphorImager. Lane 1: **V**+**L**; lane 2: **V**+2**L**; lane 3: **V**+3**L**; lane 4: **V**+4**L**; lane 5: **V**+5**L**; lane 6: 5WJ **V** (P32-labeled V1 oligonucleotide). c) Representative transmission electron micrograph (TEM) of a gold-nanoparticle-labeled **U** 5WJ in a $\mathbf{VU_5}$ complex. Scale bar: 20 nm. d) Defocused image of the same field; gold nanoparticles appear as white spheres as a result of defocusing. Scale bar: 20 nm.[14]

[*] D. Bhatia,[+] S. Mehtab,[+] R. Krishnan, Dr. Y. Krishnan
National Centre for Biological Sciences, TIFR
GKVK, Bellary Road, Bangalore, 560 065 (India)
Fax: (+91) 80-2363-6662
E-mail: yamuna@ncbs.res.in
Dr. S. S. Indi
Department of Microbiology and Cell Biology
Indian Institute of Science, Bangalore 560 012 (India)
Dr. A. Basu
National Institute of Virology
20 A, Dr. Ambedkar Road, Pune 411 001 (India)
[+] These authors contributed equally to this work.

[**] We thank Professors Ben F. Luisi, John A. Tainer, Srikanth Sastry, and S. Ramaswamy for critical comments, and G. K. Ananthasuresh and G. Krishnan for assistance with model building. This research was funded by the NSTI and DST of the Government of India, and by the DBT of the Government of India through an Innovative Young Biotechnologist Award to Y.K.

Supporting information for this article is available on the WWW under http://dx.doi.org/10.1002/anie.200806000.

etry in high yield (ca. 90%; Figure 3a,b). The [2:5:5] complex **I** was resistant to both T7 and lambda exonucleases, which indicates the presence of circularized component DNA strands and is consistent with the highly catenated nature of the putative tertiary structure adopted by the complex (Figure 3c; see also Figure 4 in the Supporting Information). Particle-sizing measurements on the [2:5:5] complex **I** by tapping-mode AFM gave a mean height distribution of (16.7 ± 2.7) nm ($n = 130$; Figure 6 in the Supporting Information). To obtain information on particle morphology, we adsorbed an aliquot of the specimen onto a carbon-coated, glow-discharged formvar support on a 400 mesh copper grid. The specimen was subjected subsequently to either platinum shadowing or negative staining with 1% uranyl acetate, and imaged by bright-field TEM under variable accelerating voltages (100/120/200 kV) by using a low-beam current. In both cases, several regular hexagonal and pentagonal features

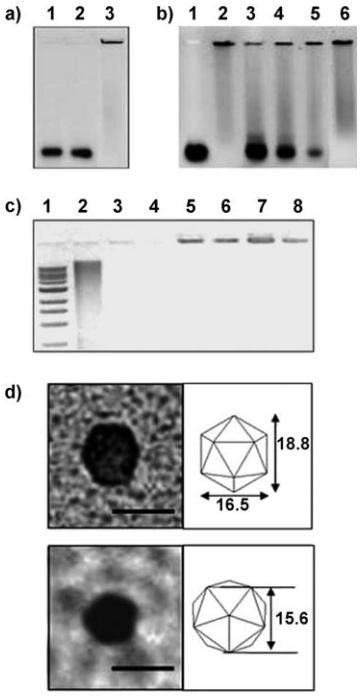

Figure 3. a) Agarose gel (0.8%) showing the formation of the [2:5:5] complex **I** from $\mathbf{VU_5}$ and $\mathbf{VL_5}$. Lane 1: ligated $\mathbf{VU_5}$; lane 2: ligated $\mathbf{VL_5}$; lane 3: the ligated [2:5:5] complex **I**. b) Agarose gel (0.8%) showing the formation of the [2:5:5] complex in the indicated stoichiometry from $\mathbf{VU_5}$ and $\mathbf{VL_5}$. Lane 1: ligated $\mathbf{VL_5}$; lane 2: the ligated [2:5:5] complex **I**; lane 3: $\mathbf{VU_5}/\mathbf{VL_5}$ (0.2:1); lane 4: $\mathbf{VU_5}/\mathbf{VL_5}$ (0.5:1); lane 5: $\mathbf{VU_5}/\mathbf{VL_5}$ (0.7:1); lane 6: $\mathbf{VU_5}/\mathbf{VL_5}$ (1:1). c) Exonuclease treatment of the ligated [2:5:5] complex on 0.8% agarose gel. Lane 1: 0.5–12 kb DNA marker; lane 2: genomic DNA from HeLa cells not treated with the exonuclease; lane 3: genomic DNA treated with 3 U of lambda exonuclease for 4 h at 37°C; lane 4: genomic DNA treated with 5 U of T7 exonuclease for 3 h at 25°C; lane 5: the ligated [2:5:5] complex, not treated with lambda exonuclease; lane 6: the ligated [2:5:5] complex treated with 3 U of lambda exonuclease for 4 h at 37°C; lane 7: the ligated [2:5:5] complex, not treated with T7 exonuclease; lane 8: the ligated [2:5:5] complex treated with 5 U of T7 exonuclease for 3 h at 25°C. d) Representative transmission electron micrographs of DNA icosahedra. Platinum-shadowed samples showing hexagonal (top left) and pentagonal (bottom left) features corresponding to C_3 and C_5 symmetries. Scale bar: 20 nm. Shown on the right are the calculated theoretical dimensions (nm).

were observed, with C_3 and C_5 symmetries, respectively (Figure 3d).

The observed cevian length of the pentagonal features was found to be (15.4 ± 0.8) nm ($n = 135$), and the observed tip-to-tip and side-to-side distances of the hexagonal features were (19.1 ± 0.6) nm ($n = 131$) and (17.3 ± 0.4) nm ($n = 128$), respectively. These dimensions were in excellent correlation with an icosahedral arrangement of the component helices in the [2:5:5] complex constructed with the software Matlab 7 (Figure 8 in the Supporting Information), for which DNA helices were assumed to be cylinders of diameter 2.3 nm. Importantly, the large numbers of hexagonal and pentagonal features indicate that the [2:5:5] complex could adopt an icosahedral tertiary structure of degree $k = 1$, as observed for several viral particles.[10,11]

To see whether the [2:5:5] complex was capable of functioning as capsules for other nanoscale entities, we mixed $\mathbf{VU_5}$ and $\mathbf{VL_5}$ in a 1:1 ratio in the presence of citrate-capped gold nanoparticles in a buffer. Following ligation with NCI, the free gold nanoparticles were separated from the [2:5:5] complex by size-exclusion chromatography on a G-75 sephadex column and dialysis. Visualization by TEM of an aliquot of the dialyzed solution of the [2:5:5] complex without staining showed that gold nanoparticles were present only in clusters of at least 6 ± 2 particles (see Figure 9 in the Supporting Information). Negative staining of the same samples with 1% aqueous uranyl acetate revealed the presence of several hexagonal and pentagonal [2:5:5] particles with a highly electron dense core under low magnification (50 kX; Figure 4a; see also Figure 10 in the Supporting Information). At higher magnification, gold nanoclusters could be visualized clearly inside [2:5:5] cages of average size (23 ± 2) nm (Figure 4a, inset). Furthermore, histograms of gold-nanoparticle sizes before and after encapsulation reveal a depletion of nanoparticles below 2.5 nm in diameter (Figure 4b,c). This result is consistent with an in-circle diameter of 2.8 nm of the triangular faces, as predicted for an icosahedral arrangement of helices in the [2:5:5] complex, and further indicates the overall effective porosity in these capsules. The minimum effective encapsulation volume per [2:5:5] complex is approximately 580 nm^3 or approximately 53% of the computed void volume. Modules $\mathbf{VU_5}$ or $\mathbf{VL_5}$ alone were incapable of encapsulating gold nanoparticles (see the Supporting Information). However, encapsulation by a defective [1:5:5] complex created through a different assembly strategy (see Figure 11 in the Supporting Information) and missing a single vertex gave an effective pore size of 3.5 nm. Thus, this assay for pore size in the bulk complex is sensitive to an overall loss of a single vertex within the structure.

Owing to the conformational flexibility of DNA junctions, 5WJs are unable to form icosahedra in the absence of prefolding. They assemble instead into 2D sheets at higher concentrations.[15] The advantage of a modular assembly strategy is that stoichiometrically well-defined closed capsules may be formed in high yield even at high concentrations as a result of the formation of prefolded intermediate modules as well as the increase in cooperativity associated with progressively higher order assembly. As also seen in viral capsid assembly, which utilizes very few repeating modules, a

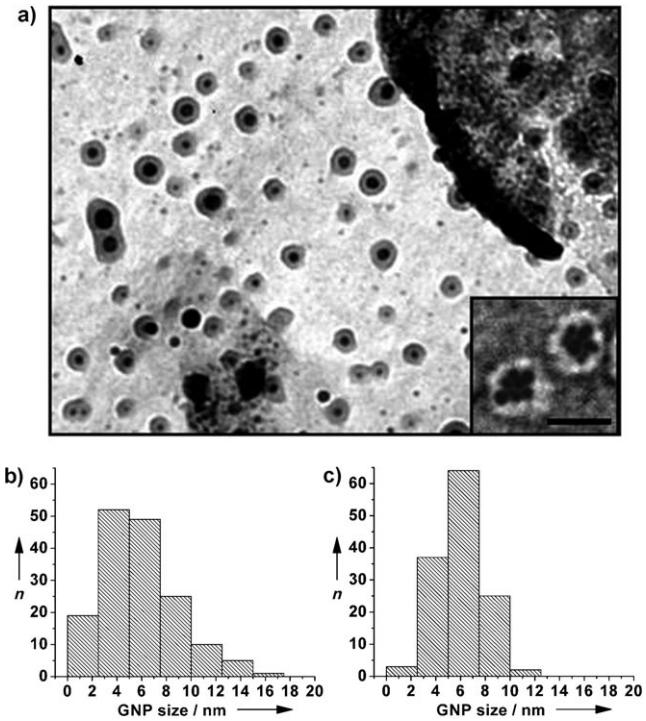

Figure 4. a) TEM image of the gold nanoparticles encapsulated within DNA icosahedra. The bright-field low-resolution TEM image shows the dense core of metallic particles within the cages. The inset shows representative high-resolution images in which the individual gold nanoparticles can be seen to be present within the icosahedral cages. Scale bar: 50 nm. b,c) Histograms showing the size-based distribution of the gold nanoparticles before (b) and after encapsulation (c).

prefolded scaffold with a defined curvature can undergo a larger number of favorable collisions that result in successful recognition events as a result of the degeneracy in the recognition sites that is associated with very few repeating modules. Modular strategies could therefore be used to construct icosahedra of even greater complexity through applications of quasiequivalence, in analogy with the assembly of large and complex viral capsids. Given the capacity of icosahedra to function as efficient nanocapsules, one could envisage targeted cargo delivery through the use of an icosahedral display of protein-binding sites on such scaffolds to create viruslike protein–DNA complexes that could be recognized by viral-entry pathways. Furthermore, the construction of an icosahedron could facilitate the formation of extended 3D frameworks owing to the well-known propensity of this polyhedron to pack.

Experimental Section

5WJs **V**, **U**, and **L** (20 μM) were constructed by annealing an equimolar mixture of 5′-phosphorylated oligonucleotides (Sigma) from 90 to 20 °C in sodium phosphate buffer. The [1:5] complexes $\mathbf{VU_5}$ and $\mathbf{VL_5}$ were created by annealing **V** and **U**/**L** in a 1:5 ratio (3.33 μM) from 45 °C to room temperature. The [2:5:5] complex **I** was formed by annealing $\mathbf{VU_5}$ and $\mathbf{VL_5}$ in 1:1 ratio (1 μM) from 45 °C to room temperature. All the samples were analyzed by electrophoresis by using either 10% PAGE (polyacrylamide gel electrophoresis) in 1X TBE buffer (TBE = Tris base (tris(hydroxymethyl)aminomethane)/boric acid/ethylenediaminetetraacetic acid (EDTA)) or 0.8% agarose in 1X TAE (TAE = Tris base/acetate/EDTA) at 4 °C. All [1:5] and [2:5:5] complexes were ligated with NCI at room temperature as described previously.[16] Gold nanoparticles of the desired sizes were synthesized by using the standard tannic acid–citrate–bicarbonate reduction method.[12,13] GNP-labeled [1:5] complexes and the [2:5:5] samples before and after GNP encapsulation were analyzed with either a JEOL 100 or a Tecnai 12 Biotwin TEM instrument operating at 80 or 100 kV. Size-exclusion chromatography was performed on a Biosep SEC 3000 column attached to a Shimadzu Prominence HPLC instrument equipped with UV and fluorescence detectors. Procedures for the exonuclease treatment of all samples are described in the Supporting Information.

All procedures and experiments are described in detail in the Supporting Information in the section Materials and Methods.

Received: December 9, 2008
Published online: February 16, 2009

Keywords: DNA · five-way junctions · nanotechnology · platonic solids · self-assembly

[1] a) J. Chen, N. C. Seeman, *Nature* **1991**, *350*, 631–633; b) F. A. Aldaye, H. F. Sleiman, *J. Am. Chem. Soc.* **2007**, *129*, 13376–13377.
[2] a) R. P. Goodman, I. A. T. Schaap, C. F. Tardin, C. M. Erben, R. M. Berry, C. F. Schmidt, A. J. Turberfield, *Science* **2005**, *310*, 1661–1665; b) C. M. Erben, R. P. Goodman, A. J. Turberfield, *Angew. Chem.* **2006**, *118*, 7574–7577; *Angew. Chem. Int. Ed.* **2006**, *45*, 7414–7417; c) R. P. Goodman, M. Heilemann, S. Doose, C. M. Erben, A. N. Kapanidis, A. J. Turberfield, *Nat. Nanotechnol.* **2008**, *3*, 93–96.
[3] a) Y. He, T. He, M. Su, C. Zhang, A. E. Ribbe, W. Jiang, C. Mao, *Nature* **2008**, *452*, 198–202; b) J. Zimmermann, M. P. J. Cebulla, S. Monninghoff, G. V. Kiedrowski, *Angew. Chem.* **2008**, *120*, 3682–3686; *Angew. Chem. Int. Ed.* **2008**, *47*, 3626–3630.
[4] Y. Zhang, N. C. Seeman, *J. Am. Chem. Soc.* **1994**, *116*, 1661–1669.
[5] a) W. M. Shih, J. D. Quispe, G. F. Joyce, *Nature* **2004**, *427*, 618–621; b) F. F. Andersen, B. Knudson, C. L. P. Oliveira, R. F. Frøhlich, D. Krüger, J. Bungert, M. Agbandje-McKenna, R. Mckenna, S. Juul, C. Veigaard, J. Koch, J. L. Rubinstein, B. Guldbrandtsen, M. S. Hede, G. Karlsson, A. H. Andersen, J. S. Pedersen, B. R. Knudsen, *Nucleic Acids Res.* **2008**, *36*, 1113–1119.
[6] J. L. Kadrmas, A. J. Ravin, N. B. Leontis, *Nucleic Acids Res.* **1995**, *23*, 2212–2222.
[7] Y. Wang, J. E. Mueller, B. Kemper, N. C. Seeman, *Biochemistry* **1991**, *30*, 5667–5674.
[8] K. J. Luebke, P. B. Dervan, *Nucleic Acids Res.* **1992**, *20*, 3005–3009.
[9] J. Qi, R. H. Shafer, *Nucleic Acids Res.* **2005**, *33*, 3185–3192.
[10] "Principles of Virus Structure": S. C. Harrison in *Field's Virology* (Eds.: D. M. Knipe, P. M. Howley), 5th ed., Lippincott Williams & Wilkins, Philadelphia, **2007**, pp. 59–98.
[11] D. D. Caspar, A. Klug, *Cold Spring Harbor Symp. Quant. Biol.* **1962**, *27*, 1–24.
[12] C. A. Mirkin, *Inorg. Chem.* **2000**, *39*, 2258–2272.
[13] D. G. Duff, A. Baiker, P. P. Edwards, *J. Chem. Soc. Chem. Commun.* **1993**, 96–98.
[14] S. Schamm, C. Bonafos, H. Coffin, N. Cherkashin, M. Carrada, A. G. Ben, A. Claverie, M. Tence, C. Colliex, *Ultramicroscopy* **2008**, *108*, 346–357.
[15] C. Zhang, M. Su, Y. He, X. Zhao, P. Fang, A. E. Ribbe, W. Jiang, C. Mao, *Proc. Natl. Acad. Sci. USA* **2008**, *105*, 10665–10669.
[16] H. B. Ghodke, R. Krishnan, K. Vignesh, G. V. P. Kumar, C. Narayana, Y. Krishnan, *Angew. Chem.* **2007**, *119*, 2700–2703; *Angew. Chem. Int. Ed.* **2007**, *46*, 2646–2649.

